Assiut University Journal of Multidisciplinary Scientific Research (AUNJMSR)
Faculty of Science, Assiut University, Assiut, Egypt.
Printed ISSN 2812-5029
Online ISSN 2812-5037
Vol. 55 (3): 751- 779 (2026)
https://aunj.journals.ekb.eg

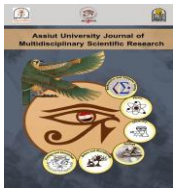

Thermodynamic and Kinetic Analysis of Marvel Grass Pyrolysis and Characterization of the Derived Biochar

Amal S. M. Gad El-hak [*a], Muhammad Abdel-Shakour [a], Abdalrahman G. Algamal [b], Abu El-Eyuoon Abu Zied Amin [c], Refaat M. Mahfouz [a]

[a]Chemistry Department, Faculty of science, Assiut University, Assiut, 71516, Egypt

[b]Egyptian Petroleum Research institute, Egypt

[c]Soil and Water Department, Faculty of Agriculture, Assiut University, Assiut, Egypt, 71526

*Corresponding author: amal011193@science.aun.edu.eg

ARTICLE INFO

Article History:
Received: 2026-04-23
Accepted: 2026-08-11
Online: 2026-08-31

Keywords:
Marvel grass; Thermogravimetric analysis; Biochar; BET surface area; Isoconversional kinetics.

ABSTRACT

Marvel grass (Dichanthium annulatum) is a perennial grass prevalent in Egypt and Africa, representing a viable source of renewable lignocellulosic biomass for sustainable energy. Its physicochemical properties were analyzed through FTIR, XRD, and SEM techniques. Thermogravimetric analysis (TGA) at heating rates of 10, 20, and 30 °C min^{-1} examined the pyrolysis behavior and determined kinetic parameters, including activation energy (Ea), frequency factor (lnA), and the conversion function (f(α)). The thermal degradation process consists of initial moisture removal followed by devolatilization linked to hemicellulose and cellulose breakdown, resulting in a carbon-rich product. Isoconversional methods indicated that pyrolysis is

multifaceted, with variable activation energy across conversions. Master plot analysis indicated that the mechanism was initially controlled by two-dimensional diffusion (D2) from 0.10 to 0.60 conversion, transitioning to three-dimensional diffusion (D3, Jander model) from 0.60 to 0.90. Negative entropy values suggested the formation of a more ordered activated complex, indicating a controlled decomposition pathway. The biochar produced was characterized using FTIR, XRD, and N_2 adsorption–desorption (BET/BJH), revealing that nitric acid modification increased the BET specific surface area from 28 to 79 $m^2\ g^{-1}$ and the total pore volume from 0.025 to 0.065 $cm^3\ g^{-1}$ while the average pore radius remained similar (18 and 17 Å for pristine and modified biochar, respectively). These findings enhance understanding of Marvel grass's thermal conversion and emphasize the modified biochar's utility for environmental and agricultural purposes.

1. INTRODUCTION

Environmental protection and fossil fuel depletion are some of the driving forces that push technological research towards the development of alternative fuels. Second-generation biofuels derived from biomass offer a sustainable alternative, able to transform an abundance into fuels with properties similar to conventional fossil fuels[1].

Biomass is a source of short-cycle carbon, where the carbon absorbed during the growth of the biomass feedstock balances with the carbon produced during its use, maintaining a balanced carbon cycle. Biomass materials are increasingly attractive renewable energy sources due to their availability, carbon neutrality, and diverse applications [2]. Grass biomass represents an abundant lignocellulosic feedstock with significant potential for thermochemical conversion and biochar production [3].

Pyrolysis is an effective thermochemical conversion process that transforms

lignocellulosic biomass into biochar, bio-oil, and gaseous products under oxygen-limited

conditions. It is crucial to note that kinetic and thermodynamic studies for the thermal

degradation of carbonaceous material are important for designing efficient and safe processes.

The devolatilization behavior of lignocellulosic biomass can be effectively investigated using thermogravimetric analysis (TG). Kinetic analysis enables the determination of the apparent activation energy (Ea), pre-exponential factor (A), and reaction model f(α), providing valuable information about the thermochemical conversion mechanism occurring during pyrolysis [4, 5].

This study aims to investigate the characteristics and kinetics that describe the thermal demposition process of marvel grass.

The aim of this work is to compare the different isoconversional methods available for kinetic analysis in detail for marvel grass and provide a basis for further applications of the thermochemical conversion of marvel grass as a potential feedstock.

2. MATERIALS AND METHODS

2.1. The Sample Preparation and Characterization

Marvel grass samples were collected from the vicinity of Assiut University, Egypt, and subsequently air-dried, ground, and stored for further analyses.

2.2. Biochar and nitrogen-enriched biochar preparation and characterization

The prepared biomass was pyrolyzed independently for four hours at 400 °C in a controlled environment. The resulting biochar was then sieved to a particle size of 1 mm after being ground in a stainless-steel grinder. A known quantity of biochar was dispersed in distilled water at a solid-to-liquid ratio of 1:10 to create a homogenous suspension in order to prepare nitrogen-enriched biochar. The mixture was then allowed to react for 48 hours after concentrated nitric acid (68%) was added at a dose of 74 mL kg^{-1} charcoal while being continuously stirred.

The process was then kept going for an extra 48 hours when a concentrated ammonia solution (25%) was added at a dose of 104 mL kg^{-1} biochar with constant stirring. In the last stage, 91 mL kg^{-1} of concentrated nitric acid was added to the biochar while being continuously stirred. After that, the mixture was allowed to air dry. In order to encourage the development of acidic nitrogen-containing functional groups on the surface of the biochar, the greater ratio of nitric acid to ammonia was purposefully maintained. This modification strategy was used to increase the biochar's chemical reactivity and surface functionality.

Nitrogen-enriched biochar was prepared using a sequential oxidation–ammoniation approach based on the principles of nitric-acid oxidation of biochar surfaces and subsequent nitrogen functionalization reported in previous studies, with modifications[6, 7].

2.3. Instrumentation

Thermogravimetric analysis (TGA) was conducted on a Mettler-Toledo (TA-TGA) in nitrogen atmosphere; the moisture zone was removed prior to kinetic study by heating the samples for 10 min at 100 oC. According to this, only active zone of hemicellulose and cellulose was subjected to kinetic analysis. Elemental analysis (C, H, N, S) was performed using a Vario-EL analyzer. Fourier transform infrared spectroscopy (FT-IR) was used to detect the functional groups of samples from 4000-400 cm−1 using a Perkin Elmer spectrometer via the KBr pellet method (Spectrum One, USA). X-ray diffraction (XRD) patterns were determined via Cu Kα X-ray radiation (Germany, λ =1.540 Å, PAN analytical X'PERT PRO). A high-resolution scanning electron microscope (HRSEM) was formfitting (JEOL, JSM [model no: 6360]) device. The textural properties of the pristine and modified biochars were characterized using a Quantachrome NOVA 3000 Series surface area and pore size analyzer (Quantachrome Instruments, USA). Prior to analysis, the biochar samples were degassed under vacuum at 250 °C for 3 h to remove physically adsorbed moisture and gases. Nitrogen adsorption–desorption isotherms were recorded at 77.3 K. The specific surface area was determined using the Brunauer–Emmett–Teller (BET) method, while the pore size distribution, pore volume, and average pore radius were calculated using the Barrett–Joyner–Halenda (BJH) method from the desorption branch of the adsorption isotherm.

2.4. Kinetic Models-Theoretical Background

For the ground marvel samples, non-isothermal thermogravimetric analysis was performed at three distinct heating rates, 10, 20 and 30^{o}C/min, using simultaneous TGA-DTG equipment; the sample was heated in a controlled nitrogen gas atmosphere to temperatures between ambient temperature and 700 ^{o}C. Firstly, 2.5 mg of every sample was heated to 100 °C in an isolated system for 10 minutes to remove moisture. Afterward, the samples were heated continuously from 100 °C to 700 °C[8]. Kinetic analysis was performed using model-free and model-fitting approaches to determine the activation energy and reaction mechanism of Marvel grass pyrolysis.

The degree of conversion (α) was calculated using Equation (1), which expresses the conversion during thermal decomposition.

$$\alpha = \frac{(m_o - m_t)}{(m_o - m_f)} \qquad (1)$$

Assuming that m_o is the sample's initial mass, m_t is its mass (at time t during degradation), m_f is its final mass, and α is the sample's conversion rate during pyrolysis. The thermal degradation of lignocellulosic biomass can be generally represented by the reaction (eq 2) [9].

$$\textit{Lignocellulosic biomass} \xrightarrow{k} \textit{Volatiles + Biochar} \qquad (2)$$

Where k is the reaction rate constant describing biomass decomposition. This process is governed by the reaction rate constant k, which can be described using the Arrhenius equation to evaluate the kinetics of thermal decomposition. In the Arrhenius equation[10] (eq 3), k is the reaction's rate constant that is dependent on temperature T.

$$k = A\, e^{-Ea/RT} \qquad (3)$$

where k is the reaction rate constant (s^{-1}), A is the pre-exponential factor (s^{-1}), Ea is the activation energy (kJ mol^{-1}), R is the universal gas constant (8.314 J mol^{-1} K^{-1}), and T is the absolute temperature (K).

According to the solid-state kinetic theory [11](eq4) is an expression for the rate of reaction that typically converts a solid state into a volatile product:

$$\frac{d\alpha}{dt} = k(T)F(\alpha) \qquad (4)$$

where k(T) is the temperature-dependent rate constant described by the Arrhenius equation. Determining the biomass's thermo kinetic behavior is crucial since it governs the decomposition process. So, in this study, model free can be calculated like linear model free such as (Flynn-wall-Ozawa technique (FWO), Kissinger – Akahira – Sunose technique (KAS), Friedman (FM)) and nonlinear model (Vyazovkin (VYZ)), Master plot as model fitting method to ascertain the reaction model.

2.4.1. Model-Free Approaches

Model-free techniques can be divided into linear model-free, such as Flynn-wall-Ozawa technique (FWO), Friedman (FM), and Kissinger. Moreover, the nonlinear model (Vyazovkin (VYZ)) and the Master plot method that is used as model-fitting method to ascertain the reaction model.

2.4.1.1. Flynn-Wall-Ozawa Ttechnique (FWO)

The FWO can be obtained as follows (eq 5)[12]:

$$\left[ln\,\beta = ln\,\frac{A.E_a}{R.g(\alpha)} - 5.335 - \frac{1.0516E_a}{RT}\right] \qquad (5)$$

2.4.1.2. Friedman Method (FM):

The Friedman differential equation is (eq 6) [13]:

$$ln\beta\,\frac{d\alpha}{dt} = ln\,[A.f(\alpha)] - E_a/RT \qquad (6)$$

2.4.1.3. Kissinger-Akahira-Sunose (KAS):

The KAS method was applied according to (eq 7)[14]:

$$ln\left(\frac{\beta}{T^2}\right) = \left(1 - \left(ln\frac{AR}{E_a g(\alpha)}\right)\right) - \frac{E_a}{RT} \qquad KAS \qquad (7)$$

2.4.1.4. Vyazovkin Method (VYZ):

Nonlinear Vyazovkin method suggested integral isoconversional approach [15-17], Ω (omega) (eq 8) minimizes the following function in order to assess the *Ea* values.

$$\Omega = \sum_{i=1}^{n}\sum_{i\neq j}^{n}\left[\frac{I(E_\alpha, T_{\alpha,j})\beta_j}{I(E_\alpha, T_{\alpha,i})\beta_i}\right] \qquad (8)$$

Where n is the number of heating rates. The temperature integralm(I) [18] (eq 9):

$$I\left(E_{\alpha,\alpha}, T_{\alpha,i}\right) = \int_0^{T_{\alpha,i}} exp\left(-\frac{E_{\alpha,\alpha}}{RT}\right) dT \qquad (9)$$

And $T_{\alpha,i}$ is a net of arbitrary temperature programs *i=1……n.*

2.4.2. Model Fitting Approach

Model-fitting methods were used to identify the most probable reaction mechanism. Formulas for f(α) and g(α) based on several solid-state reaction mechanisms [19].

2.4.2.1. Masterplot Method

The following equation was used to examine the kinetic data using the master plots approach in order to determine the reaction mechanism for marvel grass through the study of the thermal decomposition process [20].

$$\frac{g(\alpha)}{g(0.5)} = \frac{P(x)}{P(x_{0.5})} \qquad (10)$$

Where $x_{0.5}$ corresponds to the conversion degree α = 0.5. The master plot method was used to compare experimental and theoretical reaction models and identify the most probable reaction mechanism.

$$P(x) = \frac{e^{-x}}{[x(1.00198882x + 1.87391198)]} \qquad (11)$$

(eq 10) shows that when a suitable reaction model is used, the experimental value of P(x)/P(0.5) and the theoretically determined values of g(α)/g(0.5) are comparable for a given α. Thus, reaction models for solid-state reactions may be found using the master plot technique [20-22].

2.5. Thermodynamic Parameters

Thermodynamic parameters entropy ($\Delta S^{\#}$), enthalpy ($\Delta H^{\#}$), and free energy ($\Delta G^{\#}$) were calculated using eqs (12–14) [23].

$$\Delta S^{\#} = Rln\left[\frac{Ah}{exK_B T_p}\right] \qquad (12)$$

$$\Delta H^{\#} = E_a - RT_p \qquad (13)$$

$$\Delta G^{\#} = \Delta H^{\#} - T_p \Delta S^{\#} \qquad (14)$$

Where e = 2.7183 is the Neper number, χ = transition factor which is unity for mono-molecular reaction; k_B = Boltzmann constant = 1.3807×10^{-23} JK^{-1}, h = Planck's constant = 6.626×10^{-34}Js and T_p = peak temperature of DTG curve for decomposition and characterizes the highest rate of the process.

3. RESULTS AND DISCUSSION

3.1. Physicochemical Characterization

3.1.1. Elemental Analysis

Elemental analysis of marvel grass was performed to compare the relative ratio of major elements such as C, O, H, S and N. the results are listed in table 2 which shows the percentages of elemental analysis for marvel sample that shows the high content of carbon and oxygen**.**

Table 1. Elemental analysis of marvel grass shows elemental percentage.

Element	**Marvel**
Carbon	38.63%
Oxygen	53.25%
Hydrogen	6.22%
Sulfur	1.79%
Nitrogen	0.11%

The elemental composition indicates that Marvel grass contains considerable amounts of carbon (38.63%) and hydrogen (6.22%), which are favorable characteristics for thermochemical conversion and biofuel production. This suggests that marvel has a

greater organic or lignocellulosic content, making it more suitable for biochar or biofuel production. The relatively high oxygen content (53.25%) suggests the presence of abundant oxygen-containing compounds associated with cellulose and hemicellulose fractions. Such characteristics indicate that Marvel grass can serve as a promising lignocellulosic feedstock for biofuel production [24].

3.1.2. FTIR Analysis

Fig. 1a Shows FTIR spectrum of marvel grass. The FTIR spectrum revealed a broad absorption band between 3200 and 3600 cm^{-1}, characteristic of O–H stretching vibrations from alcohols and adsorbed water, confirming the presence of hydroxyl groups in cellulose and hemicellulose. Additionally, a distinct peak observed near 2900 cm^{-1} corresponds to C–H stretching vibrations from aliphatic –CH bonds, indicative of methyl and methylene functional groups. The band observed at 1730 cm^{-1} attributed to C=O stretching in carbonyl groups, possibly from carboxylic acids or esters like those in hemicellulose or pectin. A C=C stretching band at 1500–1600 cm^{-1} in aromatic rings, indicative of lignin content. The band between 1200–1450 cm^{-1} due to C–H bending and C–O stretching, associated with cellulose and hemicellulose. Peak at 1050–1150 cm^{-1} corresponds to C–O–C ether linkages, typically found in cellulose and hemicellulose structures. Bands at 600–900 cm^{-1}: Out-of-plane bending in aromatic rings, further supporting the presence of lignin[25].

3.1.3. XRD Analysis

Fig. 1b Shows XRD pattern of marvel grass powder. The broad diffraction line located at $2\theta=22°$ was indexed to (002) plane reflection of crystalline cellulose I [26]. A broad baseline and tailing after the main peak is an indication of the amorphous content, which

is usually composed of hemicellulose, lignin, and possibly residual non-cellulosic components[27]. The XRD analysis confirms the presence of crystalline cellulose, essential for thermal stability and structural integrity, significant amorphous content, which enhances chemical reactivity and biodegradability. These characteristics make the sample highly suitable for pyrolysis or gasification for energy recovery, bioethanol production due to accessible cellulose, composting or bioconversion processes [28].

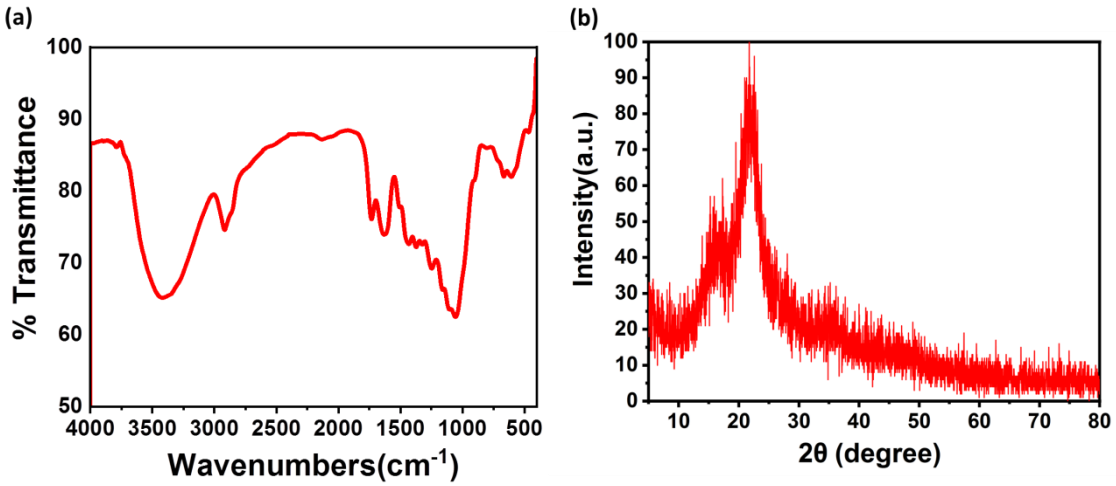

Fig. 1. (a) FTIR spectrum and (b) XRD pattern of the marvel grass.

3.1.4. SEM Analysis

Since the marvel grass sample is only dried and ground without any chemical treatment, the SEM image analysis will focus on the natural structural characteristics of the plant, such as fiber and cellulose structure, shape of plant cells after drying and grinding, Presence of cracks or fractures resulting solely from physical preparation, not chemical treatment [29]. **Fig. 2 a-f** represents SEM images of marvel grass at various magnifications (100:500X).

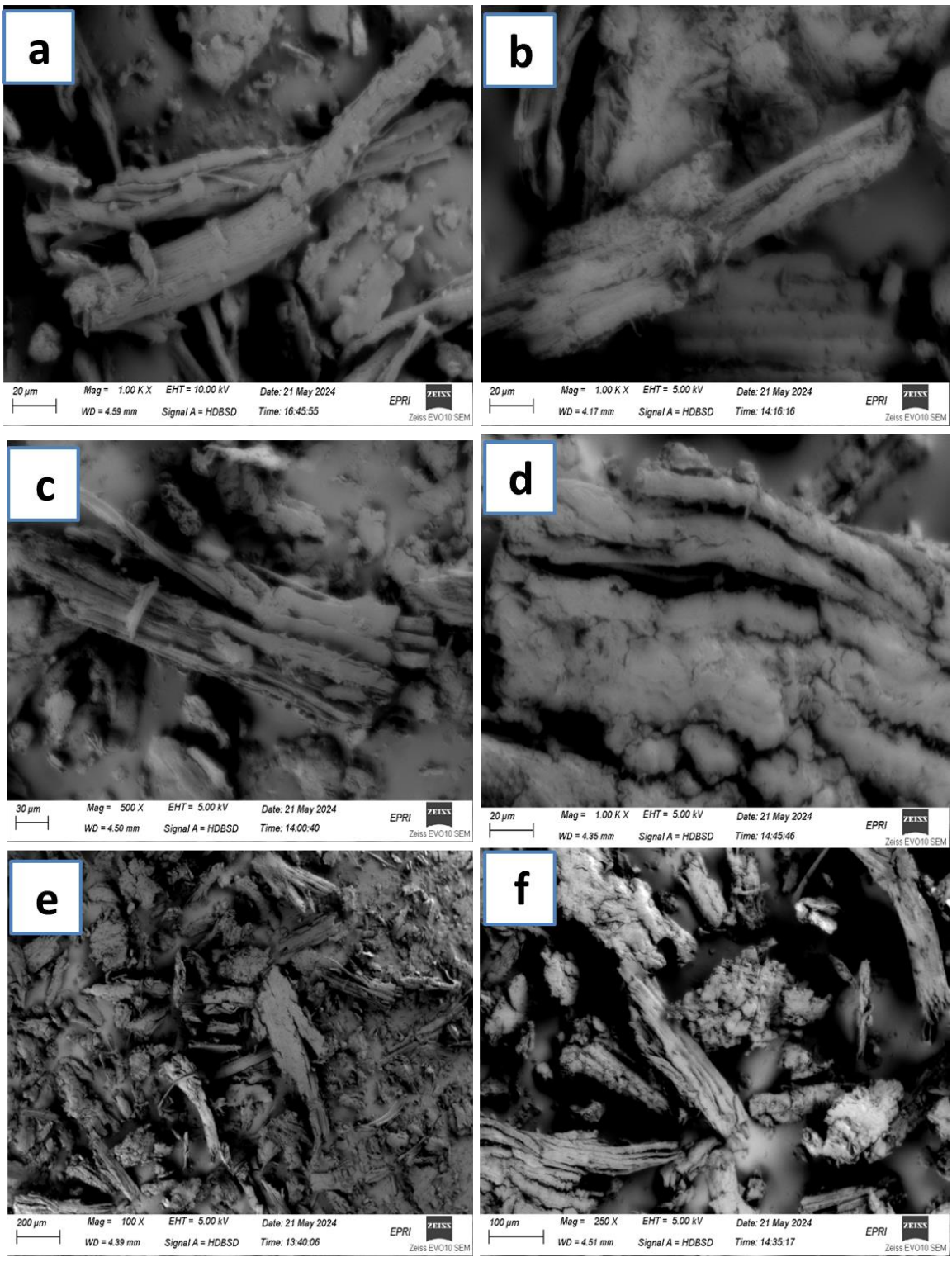

Fig. 2. SEM micrographs of marvel grass at different magnifications.

The SEM micrographs of raw Marvel grass reveal a fibrous and porous lignocellulosic structure with irregular surface morphology. The presence of natural pores and channels may facilitate heat and mass transfer during thermal conversion processes. Such structural characteristics support the suitability of Marvel grass as a potential feedstock for pyrolysis and biochar production [30].

3.2 Thermal Degradation Behavior of Marvel grass

3.2.1 TG and DTG Analysis

The thermal degradation profile of marvel grass was studied using a non-isothermal thermogravimetric approach. The TGA was operated under a nitrogen atmosphere in the temperature range of 100-700°C at the heating rates of 10, 20, and 30°C/min. The typical TG thermogram can be described by one major step in the temperature range of 200-400°C attributed to the decomposition of hemicellulose and cellulose. The degradation was limited to 20% residual weight assigned to biochar residue.

The DTG thermograms showed no lignin peak was remarkably detected in this plant.

3.2.2 Effect of Heating Rate

The effect of heating rate was studied at three dynamic rates. The thermograms demonstrated that T_{max} increases with an increasing heating rate.

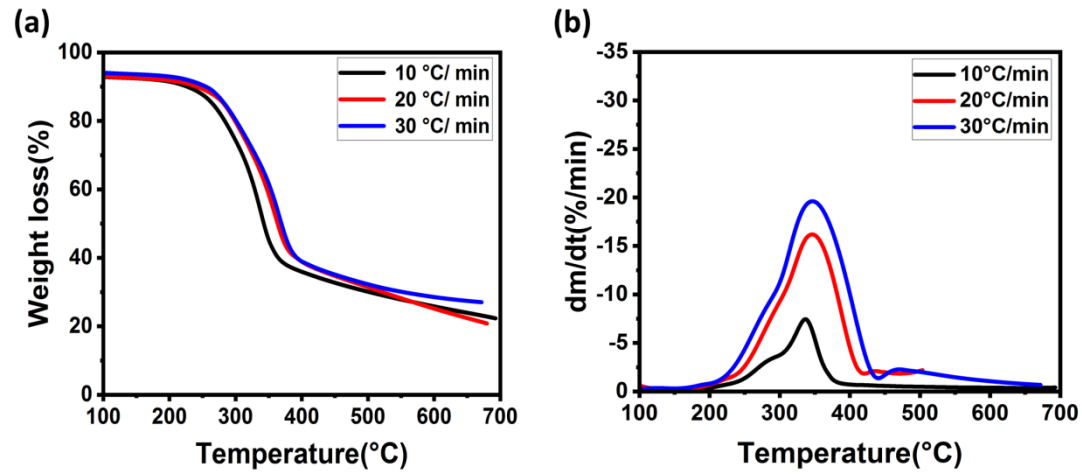

Fig. 3. (a)TG (b) DTG curves of marvel grass at different heating rates (10, 20 and 30 ^{o}C min^{-1}).

3.3 Kinetic Parameters

The accurate calculation of model-free and model-fitting equations relies on knowing the precise degree of conversion at each decomposition stage. As illustrated in **Fig. 4** for marvel grass, tracking this conversion throughout the thermal process provides the necessary data for robust kinetic analysis. The relationship between temperature and degree of conversion is crucial for the subsequent analysis of the kinetic and thermodynamic behavior of the biomass samples. As clearly shown in the figure, the decomposition rate of marvel grass increases rapidly at higher temperatures, and the onset of rapid decomposition shifts to higher temperatures as the heating rate increases, reflecting faster thermal degradation at higher heating rates. The temperature at which the degree of conversion increases sharply is seen to depend on the heating rate, shifting to higher temperatures as the heating rate increases, as expected from the faster thermal degradation at higher heating rates.

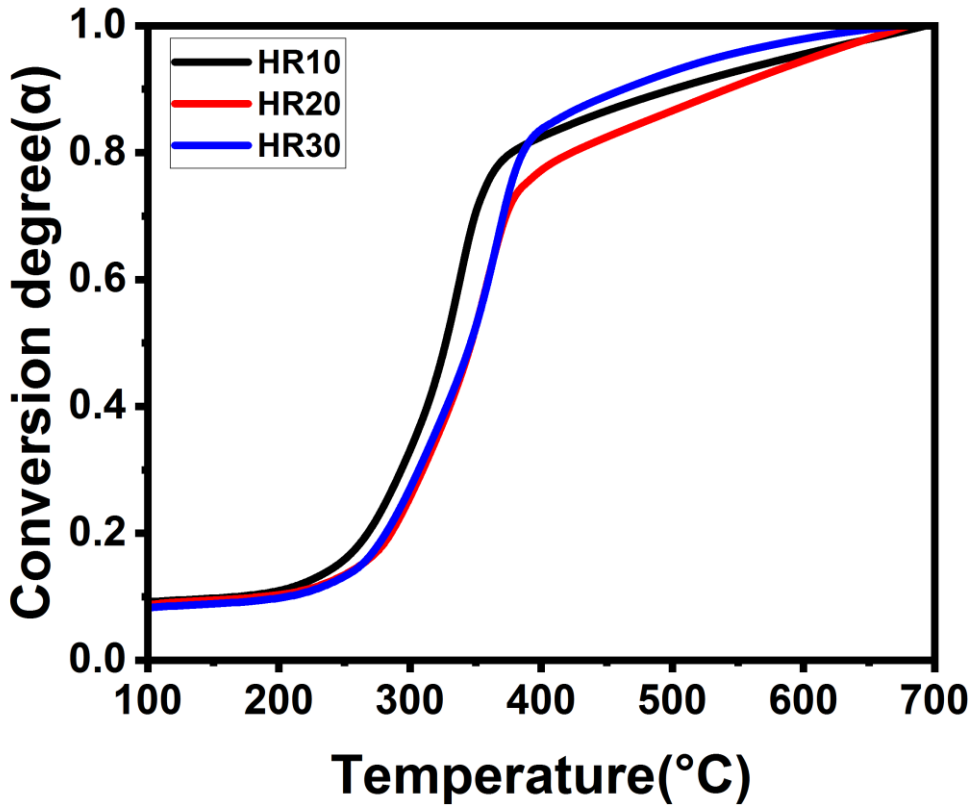

Fig. 4. Degree of conversion (α) against Temperature (^{o}C) of marvel grass at heating rates of 10, 20 and 30^{o} C min^{-1}.

3.3.1 Model Free Approach

The thermal decomposition kinetics of Marvel grass were systematically analyzed using model-free isoconversional methods, namely Flynn–Wall–Ozawa (FWO), Kissinger–Akahira–Sunose (KAS), and Friedman (FM), as presented in Fig. 5(a–d). These methods enable accurate evaluation of the activation energy without assuming a specific reaction model, which is particularly suitable for complex lignocellulosic biomass.

The FWO plots (Fig. 5a) exhibit a series of nearly parallel straight lines over a wide range of conversion degrees (α), indicating that the activation energy remains relatively stable

within specific intervals. This behavior suggests that the degradation process proceeds without abrupt mechanistic transitions, although slight deviations at higher conversion levels may be attributed to structural transformations and char formation.

The KAS plots (Fig. 5b) also show good linearity with relatively consistent slopes across different conversion degrees. The close similarity between the FWO and KAS results confirms the reliability and consistency of the calculated activation energy values. This agreement indicates that both integral methods effectively describe the overall degradation behavior and support the presence of overlapping reaction steps.

In contrast, the Friedman plots (Fig. 5c), based on the differential approach, exhibit a higher degree of data scattering. This is expected due to the sensitivity of the method to experimental noise. Nevertheless, the general linear trend confirms the validity of the kinetic analysis and provides additional insight into the local variations of the reaction mechanism during decomposition.

The variation of activation energy (Ea) with conversion degree (Fig. 5d) reveals a non-monotonic trend, characterized by an initial decrease, followed by a minimum at $\alpha \approx 0.4$–0.6, and a subsequent increase at higher conversion levels. This behavior reflects the inherent heterogeneity of lignocellulosic biomass. The higher Ea values at low conversion are attributed to the decomposition of hemicellulose, which requires relatively high energy due to its complex structure. The decrease in Ea at intermediate conversion corresponds to the degradation of cellulose, which is more thermally reactive. At higher conversion degrees, the increase in Ea is associated with lignin decomposition and the formation of thermally stable char structures.

Overall, the dependence of activation energy on conversion confirms that the thermal degradation of Marvel grass follows a heterogeneous and multi-step mechanism involving overlapping reactions. The strong agreement between FWO and KAS methods further validates the robustness of the obtained kinetic parameters, while the Friedman method provides complementary insight into the reaction complexity. These findings are crucial for optimizing pyrolysis conditions and improving biochar production from this biomass.

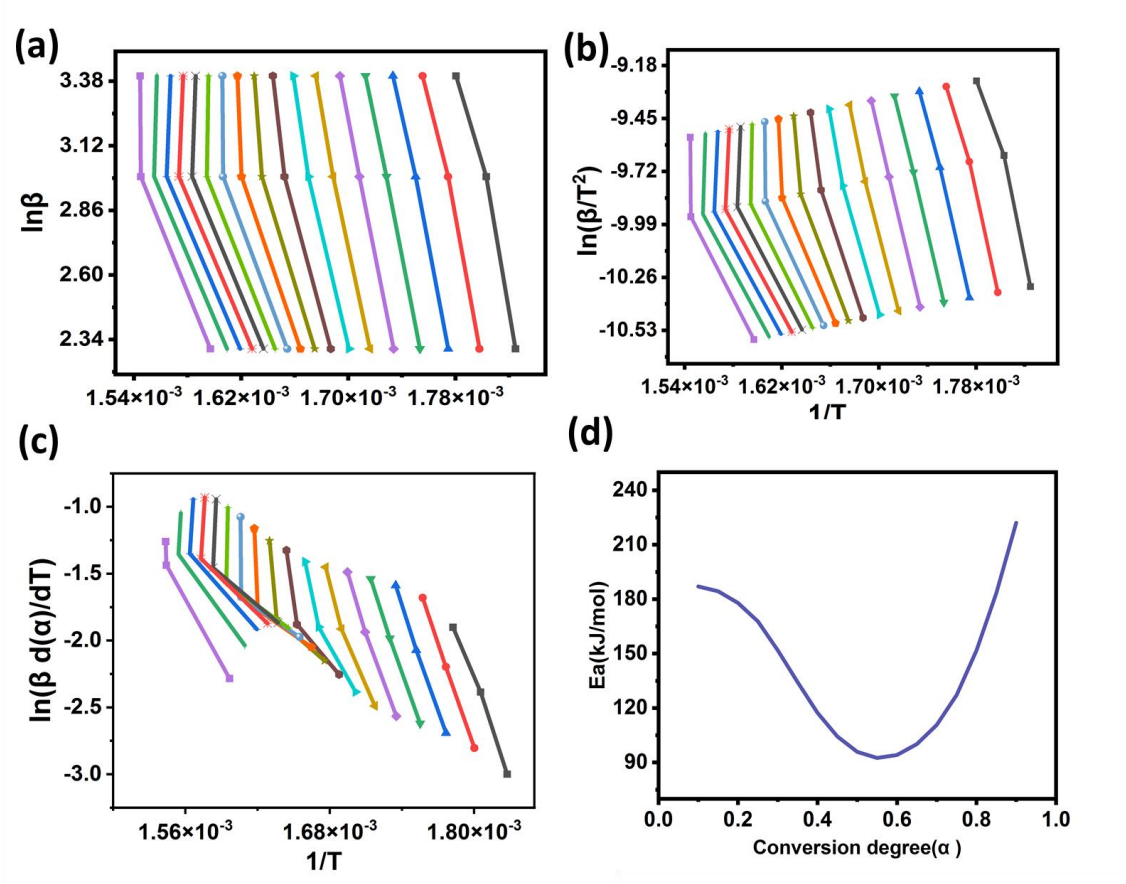

Fig. 5. Graphs of model free approaches (a) FWO method (b) KAS (C) Friedman method (d) E_a against α plot of VYZ for main step of marvel grass at heating rates of 10, 20 and 30 $^{o}C\ min^{-1}$**.**

Table 2. Activation energy (*Ea*) values of model free approaches for marvel grass's main step.

α	A (FWO) sec^{-1}	E_a(FWO) kJ/mol	E_a(KAS) kJ/mol	E_a(FM) kJ/mol	E_a(VYZ) kJ/mol
0.1	2.446E+12	168.371	168.927	179.542	179.342
0.15	1.425E+17	217.059	218.288	178.718	178.518
0.2	1.187E+13	174.354	175.514	202.806	202.606
0.25	1.217E+13	174.354	175.521	186.71	186.51
0.3	1.150E+13	174.354	175.507	132.52	132.32
0.35	1.606E+16	209.106	210.204	125.297	125.097
0.4	1.264E+16	209.106	209.647	120.983	120.783
0.45	8.696E+11	163.162	162.91	124.365	124.165
0.5	8.956E+11	163.162	162.223	79.747	79.547
0.55	1.271E+13	177.003	174.555	88.064	87.864
0.6	1.244E+13	177.003	173.78	95.96	95.76
0.65	1.032E8	117.863	114.678	105.252	105.052
0.7	1.066E8	117.863	114.275	117.125	116.925
0.75	1.093E8	117.863	114.012	129.694	129.494
0.8	1.116E8	117.863	113.873	127.489	127.289
0.85	1.137E8	117.863	113.858	178.831	178.631
0.9	1.134E8	118.002	114.82	233.657	233.457

3.3.2. Model Fitting Approach

In this work, the masterplots method (equations 10 and 11) was employed to identify the reaction models most likely to govern the kinetics of the decomposition phases. The results, as depicted in **Fig. 6** demonstrated that the models D2 and D3 were the best fits to the

experimental data of the marvel grass decomposition main step in the degradation of hemicellulose and cellulose.

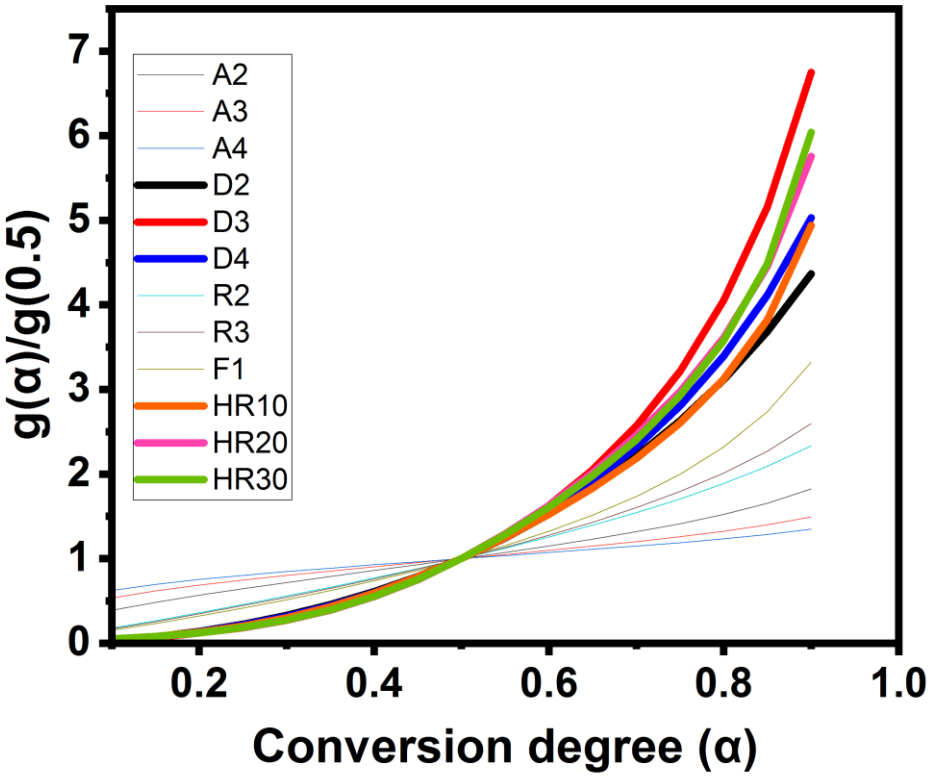

Fig. 6. Masterplot method of main step marvel grass at heating rates of 10, 20 and 30 ^{o}C min^{-1}.

3.3.3 Thermodynamic Analysis

The thermodynamic parameters of Marvel grass pyrolysis, including enthalpy change (ΔH), Gibbs free energy change (ΔG), and entropy change (ΔS), were calculated from the activation energy values obtained using the Friedman method. The calculated values at different conversion degrees are presented in Table 4.

Table 3. Parameters of thermodynamics for the decomposition of main step of marvel.

conversion (α)	E_a(FM)kJmol^{-1}	ΔH(kJmol^{-1})	ΔG(kJmol^{-1})	ΔS(kJmol^{-1} K^{-1})
0.1	179.542	174.362	174.228	0.016
0.15	178.718	173.539	173.413	0.015
0.2	202.806	197.626	197.16	0.056
0.25	186.71	181.53	181.301	0.028
0.3	132.52	127.34	127.865	-0.063
0.35	125.297	120.117	120.734	-0.074
0.4	120.983	115.804	116.478	-0.081
0.45	124.365	119.185	119.808	-0.075
0.5	79.747	74.567	75.783	-0.146
0.55	88.064	82.884	83.981	-0.132
0.6	95.96	90.781	91.768	-0.119
0.65	105.252	100.072	100.937	-0.104
0.7	117.125	111.946	112.659	-0.086
0.75	129.694	124.514	125.08	-0.068
0.8	127.489	122.309	122.935	-0.075
0.85	178.831	173.651	173.245	0.049
0.9	233.657	228.477	227.272	0.145
Average	141.574	136.394	136.744	-0.042

The ΔH values ranged from 74.57 to 228.48 kJ mol^{-1}, with an average value of 136.39 kJ mol^{-1}. The positive enthalpy values obtained throughout the conversion range indicate that the pyrolysis process is endothermic and requires continuous heat input. Furthermore, the relatively small difference between Ea and ΔH suggests that only a

limited amount of additional energy is required for the formation of the activated complex.

The Gibbs free energy values varied between 75.78 and 227.27 kJ mol^{-1}, with an average value of 136.74 kJ mol^{-1}. The positive ΔG values indicate that the formation of the activated complex is non-spontaneous and requires external energy during thermal decomposition. The entropy values ranged from −0.146 to 0.145 kJ mol^{-1} K^{-1}, with an average value of −0.042 kJ mol^{-1} K^{-1}. The predominance of negative entropy values suggests that the activated complex possesses a more ordered structure than the reactants, reflecting reduced randomness during the decomposition process. Positive entropy values observed at high conversion levels (α = 0.85–0.90) may be attributed to the decomposition of thermally resistant biomass fractions and the enhanced evolution of volatile products.

Overall, the thermodynamic results support the kinetic findings and confirm that Marvel grass pyrolysis proceeds through a complex multi-step mechanism involving significant structural transformations during thermal degradation.

3.5 Biochar Characterization

3.5.1 FTIR and X-ray analysis

The FTIR spectra of unmodified and modified Marvel biochar were recorded in the range of 4000–400 cm^{-1}, as shown in Figures 8(a,b), and the corresponding peak assignments are summarized in Tables 5 and 6.

The FTIR spectrum of the unmodified biochar exhibits a broad band around 3400 cm^{-1} attributed to O–H stretching vibrations of hydroxyl groups, which becomes less intense after pyrolysis, indicating dehydration and partial removal of surface hydroxyl functionalities. The bands observed at 2920–2850 cm^{-1} correspond to aliphatic C–H stretching vibrations, which significantly decrease in intensity, confirming the progressive decomposition of cellulose and hemicellulose during thermal treatment.

Similarly, the absorption band near 1700 cm^{-1}, assigned to C=O stretching of carbonyl-containing functional groups, shows a reduction in intensity, indicating thermal degradation of oxygenated organic moieties. In contrast, the band at approximately 1600 cm^{-1}, attributed to aromatic C=C skeletal vibrations, becomes more pronounced, suggesting an increase in aromatic condensation and the development of thermally stable carbon structures.

The persistence of bands in the region 1100–1000 cm^{-1}, associated with C–O stretching vibrations, indicates the presence of residual oxygen-containing functional groups, likely originating from incomplete decomposition of lignocellulosic components or surface functionalities.

Overall, these spectral changes confirm the transformation of raw biomass into a more carbon-rich and thermally stable biochar, consistent with the results obtained from thermal and kinetic analyses.

For the acid-modified biochar, the FTIR spectrum shows an increase in the intensity of oxygen-containing functional groups, particularly C=O (≈1710 cm^{-1}) and O–H (≈3400 cm^{-1}). This enhancement indicates surface oxidation induced by nitric acid treatment, leading to the introduction of additional carboxylic, phenolic, and hydroxyl groups. Such

functionalization increases the surface polarity and is expected to improve the adsorption and chemical reactivity of the biochar [31].

The XRD patterns of both unmodified and modified Marvel grass biochar, presented in Figures 8(c,d), indicate the presence of a predominantly amorphous carbon structure with minor crystalline mineral phases. A broad diffraction feature characteristic of amorphous carbon is observed, confirming the loss of crystalline cellulose structure during pyrolysis. In addition, weak and sharp diffraction peaks detected at approximately $2\theta \approx 26°$ and 29° are attributed to mineral components such as quartz (SiO_2) and calcite ($CaCO_3$), which originate from the inherent inorganic constituents of the biomass. The disappearance of well-defined cellulose-related crystalline peaks further confirms the thermal decomposition of lignocellulosic structure[32, 33].

Following acid modification, a slight reduction in the intensity of mineral-associated peaks is observed, which may be attributed to partial dissolution of inorganic species during nitric acid treatment. This modification also contributes to increased surface porosity and defect formation within the carbon matrix, thereby enhancing surface accessibility.

These structural transformations are consistent with the thermal degradation behavior observed in TGA analysis, confirming progressive carbonization and structural evolution of the biomass-derived biochar.

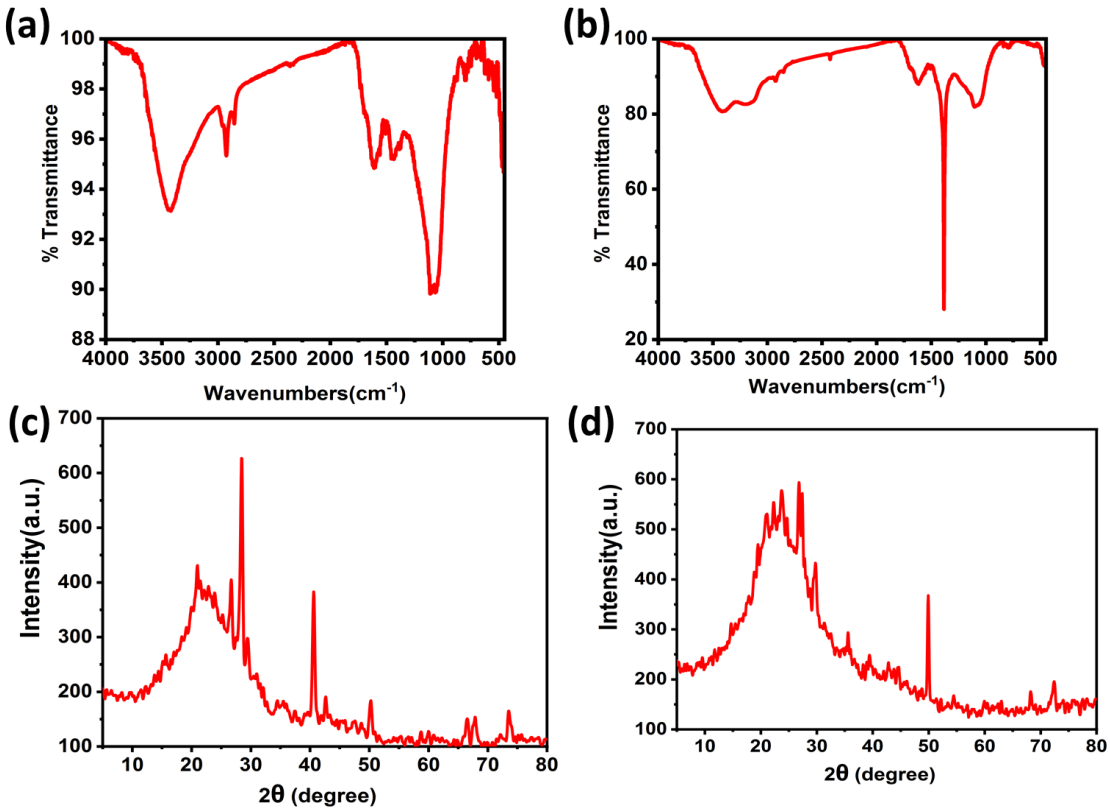

Fig. 8. FTIR spectrum of the marvel biochar sample(a) unmodified, (b) modified and XRD of marvel biochar (c)unmodified and d) modified.

Table 4. FTIR peak assignment and functional group interpretation of unmodified Marvel grass biochar

No.	Wavenumber (cm^{-1})	Vibrational mode	Functional group assignment	Interpretation
1	~3400	O–H stretching	Hydroxyl groups (phenols, alcohols, adsorbed moisture)	Indicates surface oxygenated functionalities and hydrogen bonding
2	2920	Asymmetric C–H	Aliphatic – CH_2/–CH_3	Residual lignocellulosic fragments

		stretching	groups	(cellulose/hemicellulose)
3	2850	Symmetric C–H stretching	Aliphatic $–CH_2$ groups	Presence of remaining hydrocarbon chains
4	~1700	C=O stretching	Carbonyl groups (carboxylic acids, ketones, esters)	Partially oxidized organic structures
5	~1600	Aromatic C=C stretching	Aromatic ring structures	Formation of condensed aromatic carbon network
6	~1400	O–H bending / C–H bending	Phenolic O–H / aliphatic bending	Surface functional group deformation vibrations
7	1100–1000	C–O stretching	Alcohols, ethers, esters	Residual oxygenated groups from incomplete carbonization
8	875–700	Out-of-plane C–H bending	Aromatic C–H bonds	Confirmation of substituted aromatic structures

Table 5. FTIR peak assignment and functional group interpretation of acid-modified Marvel grass biochar

Wavenumber (cm^{-1})	**Functional group**	**Assignment / interpretation**
~3400	O–H stretching	Enhanced hydroxyl and carboxylic groups due to nitric acid oxidation
2920	C–H stretching	Residual aliphatic groups from incomplete decomposition
~1710	C=O stretching	Carboxylic acids, ketones introduced via oxidation

~1600	Aromatic C=C stretching	Aromatic skeletal vibrations (carbonized structure)
~1380	O–H bending / C–N stretching	Phenolic O–H and possible nitrate-related surface functionalities
~1250	C–O stretching	Carboxylic acids, phenols, esters
~1050	C–O–C / Si–O stretching	Ether linkages or mineral-associated silicates
800–700	Aromatic C–H out-of-plane bending	Substituted aromatic ring structures

3.5.2 Textural properties of pristine and modified Marvel biochars

The textural properties of the pristine and nitric acid-modified Marvel biochar were investigated by N_2 adsorption–desorption analysis. The corresponding adsorption–desorption isotherms and BJH pore size distribution curves are presented in Figure 9(a, b), respectively, while the calculated textural properties are summarized in Table 6. From Figure 9(a) and according to the IUPAC classification, both samples exhibit Type III isotherms with no hysteresis loop, indicating weak adsorbate–adsorbent interaction and the absence of well-defined mesoporosity. The modified sample showed a significant increase in N_2 uptake compared to the non-modified sample. At P/P_0 = 1.0, the adsorption capacity increased from ~21 cc/g for MB to ~52 cc/g for MMB, corresponding to an approximately 2.5-fold increase. The similarity of the isotherm type before and after chemical modification indicates that the overall pore architecture of the biochar was preserved.

The BET results revealed that nitric acid modification markedly improved the textural properties of the biochar. The specific surface area increased from 28 $m^2\ g^{-1}$ for the

pristine biochar to 79 $m^2\ g^{-1}$ for the modified biochar. Likewise, the total pore volume increased from 0.025 to 0.065 $cm^3\ g^{-1}$**,** whereas the average pore radius remained nearly unchanged (18 and 17 Å, respectively). The substantial increase in surface area and pore volume suggests that nitric acid treatment enhanced the accessibility of the internal pore network by removing residual tar deposits and mineral impurities while creating additional oxygen-containing surface sites.

The pore size distribution curves, Figure 9(b), reveal that both samples mainly contain micropores and small mesopores in the range of 1.5–3.0 nm. The intensity of the peaks for MMB is approximately 2.5 times higher than that of MB, indicating that the modification process increased the total pore volume without altering the pore structure. Thus, the modification successfully enhanced the surface area and porosity of MB.

The BJH analysis further confirmed that both biochars retained their mesoporous characteristics after modification. The nearly constant average pore radius indicates that the oxidation treatment did not significantly alter the pore geometry but rather increased the number of accessible pores. This observation demonstrates that nitric acid treatment mainly improved the textural accessibility of the biochar without causing structural collapse [34].

These results are consistent with the FTIR results, which demonstrated the formation of additional oxygen-containing functional groups after oxidation, while the XRD patterns confirmed that the carbon matrix remained predominantly amorphous. Therefore, nitric acid modification simultaneously enhanced both the surface chemistry and the textural characteristics of the Marvel biochar. Such improvements are expected to increase its

adsorption capacity and improve its performance as a soil amendment, particularly in calcareous sandy soils where high surface area and abundant surface functional groups are desirable for nutrient retention and water-holding capacity.

Table 6. Textural properties of pristine and nitric acid-modified Marvel biochars determined from N_2 adsorption–desorption (BET/BJH) analysis.

Sample	BET surface area ($m^2\ g^{-1}$)	BJH surface area ($m^2\ g^{-1}$)	Average pore radius (Å)	Pore volume ($cm^3\ g^{-1}$)
Marvel biochar (MB)	28	17	18	0.025
Modified Marvel biochar (MMB)	79	45	17	0.065

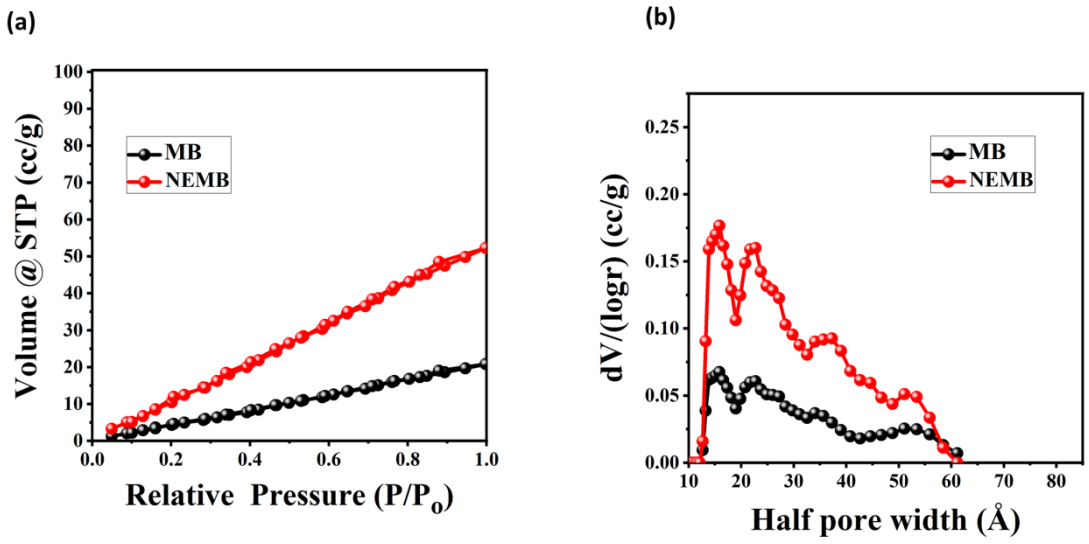

Figure 9. N_2 adsorption–desorption isotherms (a) and BJH pore size distribution curves (b) of pristine Marvel biochar (MB) and nitric acid-modified Marvel biochar (MMB).

4. CONCLUSION

The present study provides a comprehensive kinetic and thermodynamic investigation of the thermal decomposition of Marvel grass under non-isothermal conditions. The results demonstrate that the pyrolysis process proceeds through a complex multi-step mechanism, as evidenced by the variation of activation energy with conversion. The good agreement among the applied isoconversional methods confirms the reliability of the calculated kinetic parameters. Model-fitting analysis identified diffusion-controlled mechanisms (D2 and D3) as the dominant reaction models, highlighting the important role of diffusion during thermal decomposition. Thermodynamic analysis showed that the pyrolysis process is endothermic and requires external energy input, while the predominantly negative entropy values indicate the formation of a relatively ordered activated complex during most stages of decomposition.

The derived biochar was successfully characterized using FTIR, XRD, and nitrogen adsorption (BET/BJH) analyses. Nitrogen adsorption analysis demonstrated that nitric acid modification significantly increased the BET specific surface area from 28 to 79 $m^2 g^{-1}$ and enhanced the pore volume from 0.025 to 0.065 $cm^3 g^{-1}$, while the average pore radius remained nearly unchanged. These results indicate that the chemical treatment improved the textural properties of the biochar without causing substantial changes in its pore architecture. The nitrogen adsorption results are consistent with the FTIR and XRD analyses, confirming successful surface functionalization while preserving the amorphous carbon framework.

Overall, this study provides valuable insight into the pyrolysis mechanism, kinetic behavior, thermodynamic characteristics, and physicochemical properties of Marvel grass

and its derived biochar, supporting its potential as a promising lignocellulosic feedstock for thermochemical conversion and value-added biochar production.

REFERENCES

[1] S. Mahapatra, D. Kumar, B. Singh, P.K. Sachan, Biofuels and their sources of production: A review on cleaner sustainable alternative against conventional fuel, in the framework of the food and energy nexus, Energy Nexus, 4 (2021) 100036.
[2] S. Wu, K. Ye, X. Zheng, L. Zhao, Microalgal Valorization of CO2: A Sustainable Pathway to Biofuels and High-Value Chemicals, Fermentation, 11 (2025) 371.
[3] J.I. Odzijewicz, E. Wołejko, U. Wydro, M. Wasil, A. Jabłońska-Trypuć, Utilization of ashes from biomass combustion, Energies, 15 (2022) 9653.
[4] Z. Chen, M. Hu, X. Zhu, D. Guo, S. Liu, Z. Hu, B. Xiao, J. Wang, M. Laghari, Characteristics and kinetic study on pyrolysis of five lignocellulosic biomass via thermogravimetric analysis, Bioresource technology, 192 (2015) 441-450.
[5] S. Sankhla, S. Mondal, S. Neogi, Pyrolysis of cellulose nanofibers: detailed assessment of process kinetics and thermodynamic parameters, Cellulose, 30 (2023) 7695-7712.
[6] X. Zhang, S. Zhang, H. Yang, Y. Feng, Y. Chen, X. Wang, H. Chen, Nitrogen enriched biochar modified by high temperature CO2–ammonia treatment: characterization and adsorption of CO2, Chemical Engineering Journal, 257 (2014) 20-27.
[7] B. Li, K. Li, Effect of nitric acid pre-oxidation concentration on pore structure and nitrogen/oxygen active decoration sites of ethylenediamine-modified biochar for mercury (II) adsorption and the possible mechanism, Chemosphere, 220 (2019) 28-39.
[8] N.M. Azme, M. Murshed, Treatability of stabilize landfill leachate by using pressmud ash as an adsorbent, in: IOP Conference Series: Earth and Environmental Science, IOP Publishing, 2018, pp. 012041.
[9] A.A.D. Maia, L.C. de Morais, Kinetic parameters of red pepper waste as biomass to solid biofuel, Bioresource technology, 204 (2016) 157-163.
[10] R.-L. Du, K. Wu, D.-A. Xu, C.-Y. Chao, L. Zhang, X.-D. Du, A modified Arrhenius equation to predict the reaction rate constant of Anyuan pulverized-coal pyrolysis at different heating rates, Fuel Processing Technology, 148 (2016) 295-301.
[11] M. Pijolat, F. Valdivieso, M. Soustelle, Experimental test to validate the rate equation "dα/dt= kf (α)" used in the kinetic analysis of solid state reactions, Thermochimica Acta, 439 (2005) 86-93.
[12] K. Slopiecka, P. Bartocci, F. Fantozzi, Thermogravimetric analysis and kinetic study of poplar wood pyrolysis, Applied Energy, 97 (2012) 491-497.
[13] L. Tian, B. Shen, H. Xu, F. Li, Y. Wang, S. Singh, Thermal behavior of waste tea pyrolysis by TG-FTIR analysis, Energy, 103 (2016) 533-542.
[14] A.C.R. Lim, B.L.F. Chin, Z.A. Jawad, K.L. Hii, Kinetic analysis of rice husk pyrolysis using Kissinger-Akahira-Sunose (KAS) method, Procedia engineering, 148 (2016) 1247-1251.
[15] S. Vyazovkin, A unified approach to kinetic processing of nonisothermal data, International journal of chemical kinetics, 28 (1996) 95-101.
[16] S. Vyazovkin, D. Dollimore, Linear and nonlinear procedures in isoconversional computations of the activation energy of nonisothermal reactions in solids, Journal of chemical information and computer sciences, 36 (1996) 42-45.
[17] S. Vyazovkin, N. Sbirrazzuoli, Isoconversional kinetic analysis of thermally stimulated processes in polymers, Macromolecular Rapid Communications, 27 (2006) 1515-1532.

[18] J. Cai, F. Yao, W. Yi, F. He, New temperature integral approximation for nonisothermal kinetics, AIChE Journal, 52 (2006) 1554-1557.
[19] C.N. Arenas, M.V. Navarro, J.D. Martínez, Pyrolysis kinetics of biomass wastes using isoconversional methods and the distributed activation energy model, Bioresource technology, 288 (2019) 121485.
[20] F.J. Gotor, J.M. Criado, J. Malek, N. Koga, Kinetic analysis of solid-state reactions: the universality of master plots for analyzing isothermal and nonisothermal experiments, The journal of physical chemistry A, 104 (2000) 10777-10782.
[21] A. Marini, V. Berbenni, M. Pegoretti, G. Bruni, P. Cofrancesco, C. Sinistri, M. Villa, Drug-excipient compatibility studies by physico-chemical techniques; the case of atenolol, Journal of thermal analysis and calorimetry, 73 (2003) 547-561.
[22] C. Doyle, Estimating isothermal life from thermogravimetric data, Journal of Applied Polymer Science, 6 (1962) 639-642.
[23] W. Nong, X. Chen, L. Wang, J. Liang, L. Zhong, Z. Tong, Nonisothermal decomposition kinetics of abietic acid in argon atmosphere, Industrial & engineering chemistry research, 50 (2011) 13727-13731.
[24] M.F. Llorente, J.C. García, Concentration of elements in woody and herbaceous biomass as a function of the dry ashing temperature, Fuel, 85 (2006) 1273-1279.
[25] R. Md Salim, J. Asik, M.S. Sarjadi, Chemical functional groups of extractives, cellulose and lignin extracted from native Leucaena leucocephala bark, Wood Science and Technology, 55 (2021) 295-313.
[26] H.J. Kim, W.J. Lee, The influence of cellulose nanocrystal characteristics on regenerative silk composite fiber properties, Materials, 16 (2023) 2323.
[27] E.S. Madivoli, Development of cellulose-chitosan silver nanocomposites films for wound dressing applications, in, JKUAT-IBR, 2021.
[28] A.O. Adeoye, O.S. Lawal, R.O. Quadri, D. Malomo, M.T. Aliyu, G.E. Dang, E.O. Emojevu, M.J. Maikato, M.G. Yahaya, O.O. Omonije, Sustainable energy via thermochemical and biochemical conversion of biomass wastes for biofuel production, in: Transportation Energy and Dynamics, Springer, 2023, pp. 245-306.
[29] M. Jonoobi, R. Oladi, Y. Davoudpour, K. Oksman, A. Dufresne, Y. Hamzeh, R. Davoodi, Different preparation methods and properties of nanostructured cellulose from various natural resources and residues: a review, Cellulose, 22 (2015) 935-969.
[30] C. Luo, R. Wightman, E. Meyerowitz, S.K. Smoukov, A 3-dimensional fibre scaffold as an investigative tool for studying the morphogenesis of isolated plant cells, BMC Plant Biology, 15 (2015) 211.
[31] A.K. Badawi, R. Hassan, B. Ismail, Biochar-supported photocatalysts for microplastics removal: mechanisms, material design, and pathways towards real-world applications, RSC advances, 16 (2026) 17039-17062.
[32] S.M. Ismail, IMPACT OF FEEDSTOCK TYPE AND PYROLYSIS TEMPERATURE ON BIOCHAR PROPERTIES AND SOIL PHYSIOCHEMICAL CHARACTERISTICS IN El-HAMMAM REGION, EGYPT, Egyptian Journal of Desert Research, 75 (2025) 189-224.
[33] J. Bourke, Preparation and Properties of Natural, Demineralized, Pure, and Doped Carbons from Biomass; Model of the Chemical Structure of Carbonized Charcoal, in, The University of Waikato, 2007.
[34] G. Leofanti, M. Padovan, G. Tozzola, B. Venturelli, Surface area and pore texture of catalysts, Catalysis today, 41 (1998) 207-219.